

Discovery and Timing analysis of new pulsars in globular cluster NGC 5024: new observations from FAST

YUJIE LIAN,^{1,2} ZHICHEN PAN^{*},^{3,4,5} HAIYAN ZHANG[†],^{3,4,5} P. C. C. FREIRE,⁶ SHUO CAO[‡],^{1,2} AND LEI QIAN^{3,4,5}

¹*Institute for Frontiers in Astronomy and Astrophysics, Beijing Normal University, Beijing 102206, China;*

²*Department of Astronomy, Beijing Normal University, Beijing 100875, China;*

³*National Astronomical Observatories, Chinese Academy of Sciences, 20A Datun Road, Chaoyang District, Beijing, 100101, China;*

⁴*CAS Key Laboratory of FAST, National Astronomical Observatories, Chinese Academy of Sciences, Beijing 100101, China;*

⁵*College of Astronomy and Space Sciences, University of Chinese Academy of Sciences, Beijing 100049, China;*

⁶*Max-Planck-Institut für Radioastronomie, Auf dem Hügel 69, D-53121 Bonn, Germany*

ABSTRACT

NGC 5024 (M53) is the most distant globular cluster (GC) with known pulsars. In this study, we report the discovery of a new binary millisecond pulsar PSR J1312+1810E (M53E) and present the new timing solutions for M53B to M53E, based on 22 observations from the Five-hundred-meter Aperture Spherical radio Telescope (FAST). These discoveries and timing work benefit from FAST's high sensitivity. We find that M53C is the only isolated millisecond pulsar known in this distant globular cluster, with a spin period of 12.53 ms and spin period derivative of $5.26 \times 10^{-20} \text{ s s}^{-1}$. Our results reveal the orbital periods of 47.7, 5.8, and 2.4 days for M53B, D, and E, respectively. The companions, with a mass of 0.25, 0.27, and 0.18 M_{\odot} , respectively, are likely to be white dwarf stars; if they are extended objects, they don't eclipse the pulsars. We find no X-ray counterparts for these millisecond pulsars in archival *Chandra* images in the band of 0.3–8 keV. The characteristics of this pulsar population are similar to the population of millisecond pulsars in the Galactic disk, as expected from the low stellar density of M53.

Keywords: Radio telescopes(1360); Binary pulsars(153); Millisecond pulsars(1062); Globular star clusters(656)

1. INTRODUCTION

Globular clusters have such extraordinarily dense stellar environments that collisions and interactions between stars are very likely over their lifetimes. For this reason, they form unusually large numbers of low-mass X-ray binaries (LMXBs) and the latter's evolutionary products, millisecond pulsars (MSPs) per unit stellar mass (Clark 1975; Katz 1975). The LMXBs form when a member of a binary is exchanged by a lone neutron star in an *exchange interaction* (Sigurdsson & Phinney 1993).

For this reason, GCs are excellent places to search for MSPs. Following the discovery of first GC pulsar PSR B1821–24A in the GC M28 (Lyne et al. 1987),

288 pulsars in 38 GCs have been reported until 2023 May¹. This population is very different from the general pulsar population: The ATNF pulsar catalog has reported 533 MSPs with a spin period shorter than 20 ms (Manchester et al. 2005)², which are less than 16% of the total pulsar population. Meanwhile, in GCs this number is 259, about 90 % of the total. In GCs, $\sim 56\%$ of pulsars are in binary systems. Some of these pulsars can be very unusual, including the fastest spinning pulsar J1748–2446ad (spin period 1.39595 ms; Hessels et al. 2006) and the MSPs with eccentric orbits and massive companions (e.g., PSR J0514–4002A, which has an orbital eccentricity of 0.89 and a companion mass of $1.22^{+0.06}_{-0.05} M_{\odot}$; Ridolfi et al. 2019), which are

¹ * Equal contribution; panzc@bao.ac.cn

² † Equal contribution; hyzhang@bao.ac.cn

³ ‡ caoshuo@bnu.edu.cn

¹ <http://www.naic.edu/~pfreire/GCpsr.html>

² <https://www.atnf.csiro.au/research/pulsar/psrcat/>

quite unlike the orbital eccentricities and companions to MSP binaries observed in the Galactic disk.

As essential targets for searching pulsars, a number of GCs have been continuously monitored by the Five-hundred-meter Aperture Spherical Radio Telescope (FAST; Nan et al. 2011; Jiang et al. 2019, 2020; Pan et al. 2020; Wang et al. 2020). The FAST GC pulsar survey was started in 2018 and has reported 43 new pulsars in 12 GCs³. Most new discoveries are binary pulsars (33 out of 43), except in NGC6517 (2 out of 13; only NGC 6517J, and possibly 6517N are binaries).

NGC 5024 (M53, $\alpha = 13^{\text{h}}12^{\text{m}}55.3^{\text{s}}$, $\delta = +18^{\circ}10'05''$) is located in the intermediate Galactic halo at a Heliocentric distance of $R_{\text{Sun}} = 17.9$ kpc and a galactocentric distance of $R_{\text{gc}} = 18.4$ kpc (Harris 1996, 2010), it is the most distant GC with known pulsars. Also, with a central density of $\rho_c \sim 1.2 \times 10^3 L_{\odot} \text{pc}^{-3}$ it is the least dense of all GCs with pulsars. Furthermore, with $[\text{Fe}/\text{H}] \sim -2.10$, it is among the most metal-poor GCs in the Galaxy (Harris 1996, 2010).

Before this study, four pulsars (including 3 MSPs) have been reported, with a dispersion measure (DM) of ~ 25 pc cm⁻³. The first binary pulsar in M53, B1310+18A (M53A), was discovered using the Arecibo 305-m radio telescope, on a band 8 MHz wide centered on 430 MHz (Kulkarni et al. 1991). Its spin period (P) and DM value are ~ 33 ms and 24.0 pc cm⁻³, respectively; it is a binary pulsar in a 256-day orbit with a low-mass ($0.35 M_{\odot}$) **companion. Until now, no phase-coherent timing solution has been published for this pulsar.** More recently, three new MSPs (PSRs J1312+1810B, C and D, henceforth M53B to D) were discovered by FAST, all significantly fainter than M53A (Pan et al. 2021), but no timing solutions were published for these pulsars. These discoveries show that, with the high sensitivity of FAST, we can discover significant numbers of pulsars, even in very distant GCs like M53. These discoveries will help us better characterize the distribution of MSPs in globular clusters, especially for those with very low metallicities.

In section 2, we describe our 2 years of FAST observations and how the resulting data were reduced. In section 3, we present the results of our observations - the discovery of M53E and the determination of timing solutions for all pulsars - and discuss their implications. We summarize our findings in section 4.

Using FAST data, we have also derived a phase-coherent timing solution for M53A, and have extended it to the early 1990's using

archival Arecibo data, obtaining very precise spin, astrometric and orbital parameters. However, some archival data has not yet been fully analyzed. The results of this work will be published by Lian et al. (in prep).

2. OBSERVATION AND DATA REDUCTION

The tracking observation of M53 was initiated on November 30th 2019, as the pilot survey for the FAST GC pulsar survey and SP² project⁴ (Pan et al. 2021).

For this observation, we used the center beam of the FAST 19-beam L-band receiver, which has a beam size of $\sim 3'$ and covers a frequency range of 1.0-1.5 GHz. The data were 8-bit sampled for two polarizations and channeled into 4096 channels (0.122 MHz channel width), the resulting power spectra were summed every 49.152 μs . The pulsars, M53B to D were discovered in this observation, with dispersion measures (DMs) of 26.0, 26.2, 24.6, and 25.9 pc cm⁻³ respectively. The timing observations were then carried out until 2022, with the same receiver and back-end setup as for the discovery observation, which is suitable for the analysis of multiple pulsars and allows additional discoveries; their details are presented in Table 1.

This table lists the search sensitivity for these observations. This was calculated using the radiometer equation (Lorimer & Kramer 2004):

$$S_{\text{min}} = \beta \frac{(S/N_{\text{min}})T_{\text{sys}}}{G\sqrt{n_{\text{p}}T_{\text{obs}}\Delta f}} \sqrt{\frac{W}{P-W}}, \quad (1)$$

where β is the sampling efficiency and equals 1 for our 8-bit recording system, the minimum signal-to-noise (S/N) ratio $(S/N)_{\text{min}}$ is 10, the system temperature (T_{sys}) is 24 K, the antenna gain (G) is 16 K Jy⁻¹, the number of polarizations (n_{p}) is 2. T_{obs} is the integration time (in seconds) and Δf is the bandwidth in MHz, for this survey it is 300 MHz. The W and P are pulse width and period, respectively, and we take 10% for W/P .

In order to search for additional pulsars, the search on timing observation data was done on all the data with the Pulsar Exploration and Search TOolkit (PRESTO, Ransom et al. 2001, 2002, 2003)). The acceleration search with PRESTO's *accelsearch* routine was first without acceleration ($z_{\text{max}} = 0$) and then with a middle acceleration ($z_{\text{max}} = 200$). The parameter z_{max} represents the maximum number of Fourier bins that the signal can drift (linearly with time) in the power spectra (e.g., due to orbital motion or pulsar spin down over the course of the observation, see e.g., Ransom et al. 2002).

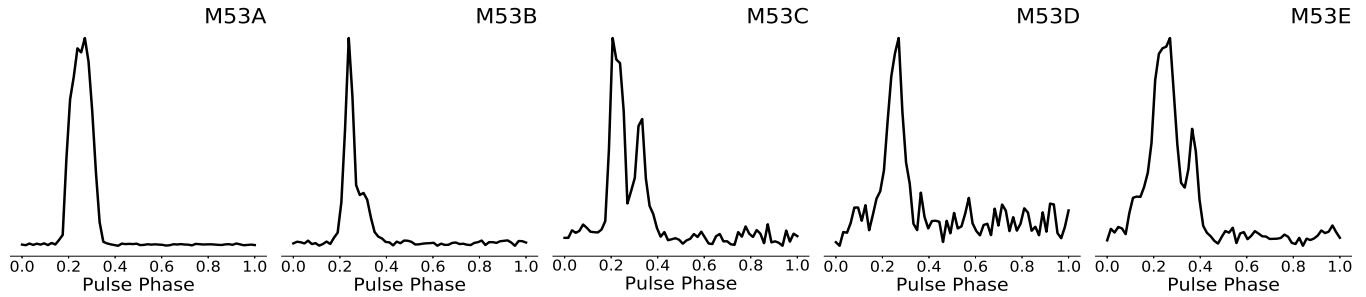
³ <https://fast.bao.ac.cn/cms/article/65/>

⁴ Search of Pulsars in Special Population, <https://crafts.bao.ac.cn/pulsar/SP2/>

Table 1. Observation details.

Date (yyyy-mm-dd)	MJD	Observation length (min)	M53D Detected ¹ Y/N	Sensitivity μJy
2019 Sep 30	58817	300	Y	0.48
2020 Oct 26	59148	300	Y	0.48
2020 Nov 19	59172	300	Y	0.48
2020 Nov 20	59173	300	Y	0.48
2020 Nov 21	59174	300	Y	0.48
2020 Nov 23	59176	300	Y	0.48
2020 Nov 25	59178	300	Y	0.48
2020 Dec 04	59187	300	N	0.48
2020 Dec 28	59211	300	N	0.48
2021 Jan 08	59222	240	N	0.54
2021 Feb 12	59257	300	Y	0.48
2021 Feb 13	59258	300	Y	0.48
2021 Jun 05	59370	288	N	0.49
2021 Jun 11	59376	180	N	0.62
2021 Sep 20	59477	300	Y	0.48
2022 Feb 24	59634	180	Y	0.62
2022 Mar 06	59644	180	N	0.62
2022 Mar 08	59646	180	N	0.62
2022 Mar 23	59661	150	Y	0.68
2022 Mar 24	59662	186	Y	0.61
2022 Mar 28	59666	120	N	0.76
2022 Apr 05	59674	58	Y	1.09

¹ M53A to C and E can be found in every observation. For M53D detection, its signal can be seen by folding data with timing solution.

**Figure 1.** Integrated pulse profiles by summing all detections. All profiles are for 64 bins.

To search for short-orbit pulsars, the data were also separated into 1-hr segments, which were then searched separately. This resulted in the discovery of M53E, which is a binary pulsar in a 2.4-day orbit. The signal of this pulsar was later recovered in the 2019 data. Because the observation time is $\sim 10\%$ of the orbital period, it was missed in the previous search. Its discovery indicates that the 10% orbital period can be the limitation for acceleration searches, as already extensively discussed in the literature. To find short orbital period binaries, the search should either be done with short observations or new methods (e.g., jerk search (Andersen & Ransom 2018)) should be employed.

We used the `fitorb.py` routine⁵ to obtain the initial orbital parameters for the binary pulsars. From our detections, we derived pulse times of arrival (ToAs) by cross-correlating the pulse profiles against a high-S/N template, which was obtained from fitting a set of Gaussian curves to the best detections. For the subsequent analysis of the ToAs, the TEMPO pulsar timing package (Nice et al. 2015)⁶ was carried out. With the latter program, we used the DRACULA script⁷ (Freire et al. 2018) to derive phase-connected timing solutions for all the pulsars. As seen from Table 1, the gap between some observations can be one month or even much longer;

⁵ <https://github.com/scottransom/presto/blob/master/bin/fitorb.py>

⁶ <http://tempo.sourceforge.net>

⁷ <https://github.com/pfreire163/Dracula>

Table 2. Timing solutions for previously discovered pulsars M53B to D and new pulsar M53E. For M53D and E, the eccentricity is derived from the ELL1 parameters^a.

Pulsar name	M53B	M53C	M53D	M53E
MJD range	58817–59674	58817–59674	58817–59674	58817–59674
Reference epoch (MJD)	59477.1528	59477.1528	59477.1528	59477.1528
Number of TOAs	344	250	66	319
EFAC	1.153	1.385	1.065	1.028
Timing residual r.m.s. (μ s)	19.24	88.57	53.23	52.98
Reduced χ^2	1	1	1	1
Solar System ephemeris model	DE440	DE440	DE440	DE440
Binary model	DD	—	ELL1	ELL1
Measured quantities				
Right Ascension, α (J2000)	13:12:54.7219(1)	13:12:55.6624(3)	13:12:55.6338(6)	13:12:55.8311(4)
Declination, δ (J2000)	+18:10:03.231(3)	+18:10:09.549(9)	+18:09:55.05(2)	+18:10:17.233(7)
Pulse Frequency, f (Hz)	160.19831544487(2)	79.77612072867(4)	164.7517730112(2)	251.75352627488(9)
Pulse Frequency Derivative, \dot{f} (s^{-2})	$4.48(1) \times 10^{-16}$	$-3.35(2) \times 10^{-16}$	$-6.14(7) \times 10^{-16}$	$4.80(5) \times 10^{-16}$
Dispersion measure, DM (cm^{-3} pc)	25.960(1)	26.194(6)	24.61(1)	25.879(5)
Orbital Period, P_b (day)	47.6773506(1)	—	5.75023947(8)	2.43137859(1)
Projected Semi-major Axis, x (lt-s)	22.616556(2)	—	5.91397(1)	2.371683(5)
Orbital eccentricity, e	0.0132417(2)	—	$1.4(4) \times 10^{-5a}$	$0.9(5) \times 10^{-5a}$
Longitude of periastron, ω (deg)	26.8885(6)	—	—	—
Epoch of passage at Periastron, T_0 (MJD)	59653.08363(8)	—	—	—
Epoch of passage at Ascending Node, T_{asc} (MJD)	—	—	59259.173859(3)	59643.937510(2)
EPS1	—	—	$1.2(4) \times 10^{-5}$	$0.8(5) \times 10^{-5}$
EPS2	—	—	$0.6(5) \times 10^{-5}$	$0.5(5) \times 10^{-5}$
Derived quantities				
Spin Period, P (ms)	6.2422628928589(7)	12.535079305264(6)	6.069737409941(8)	3.972138999587(1)
1st Spin Period Derivative, \dot{P} ($s s^{-1}$)	$-1.746(4) \times 10^{-20}$	$5.26(3) \times 10^{-20}$	$2.26(3) \times 10^{-20}$	$-7.58(8) \times 10^{-21}$
Mass Function, $f_{(M_p)}$ (M_\odot)	0.005464887(1)	—	0.00671726(5)	0.00242321(1)
Minimum companion mass, $M_{c,min}$ (M_\odot)	0.2455	—	0.2650	0.1824
Angular offset from centre in α , θ_α (arcmin)	-0.1261	+0.0974	+0.0913	+0.1374
Angular offset from centre in δ , θ_δ (arcmin)	-0.0363	+0.0691	-0.17238	+0.1971
Total angular offset from centre, θ_\perp (arcmin)	0.1312	0.1195	0.1951	0.2403
Total angular offset from centre, θ_\perp (core radii)	0.3750	0.3413	0.5573	0.6865
Projected distance from centre, r_\perp (pc)	0.7063	0.6428	1.0497	1.2929

this sparsity made it impossible to determine the timing solutions of pulsars M53B to E without recourse to DRACULA.

3. RESULTS AND DISCUSSION

In Table 2, we present the timing solutions for M53B to E. In Fig. 2, we show the post-fit timing residuals with all of the TOAs, obtained by these solutions. The fact that these show no trends indicates that the solutions provide a good description of the ToAs.

3.1. Properties of pulsars in M53

M53A is a relatively slow 33 ms pulsar, in a rather wide 256-day orbit. All new pulsars are significantly fainter than the previously known pulsar M53A, **spin faster and, for those in binaries, have shorter orbital periods.** M53B, the second brightest pulsar known in this cluster, is an MSP with $P = 6.24$ ms in a 47.7-day, mildly eccentric ($e = 0.0132$) binary system with a low-mass companion: assuming a pulsar mass of $1.4 M_\odot$, the minimum companion mass ($M_{c,min}$) is $0.246 M_\odot$.

M53C is much fainter than M53B. It is an isolated MSP with $P = 12.53$ ms, which helped detecting it in our observations. M53D is the faintest pulsar with possi-

ble interstellar scintillation. It is an MSP with $P = 6.07$ ms and a low-eccentricity orbit ($e \sim 0.000014(4)$) with a period of 5.75 d, again with a low-mass companion (with the assumptions above, $M_{c,min} = 0.265 M_\odot$). With FAST, we can detect M53B, C, and E in each observation; the detection rate of M53D is $\sim 64\%$. Finally, our newly discovered pulsar, M53E, is a 3.97-ms pulsar in a 2.43-day, low-eccentricity orbit, again with a low-mass companion $M_{c,min} = 0.182 M_\odot$.

Fig. 3 displays the positions of **M53A to E** in the cluster. All the new discoveries are located within $0.24'$ from the centre of M53, well within the core; in principle, the beam size of $3'$ should allow discoveries significantly farther out, at least to $1.5'$, which is already beyond the half-light radius. Thus, the strong concentration of new discoveries in the core is not an effect of the small beam size. The positions of six bright X-ray sources in M53 detected by *Chandra X-ray Observatory* (CXO) are presented as red circles (Zhao & Heinke 2022). Only one source (number 4) is located within the core region. With our best-fitted positions with 1σ uncertainty ($\sim 10^{-2}$ arcsec for RA and Dec), no relevant X-ray counterparts of M53B to E have been found. An unabsorbed X-ray luminosity for the six sources is within the range

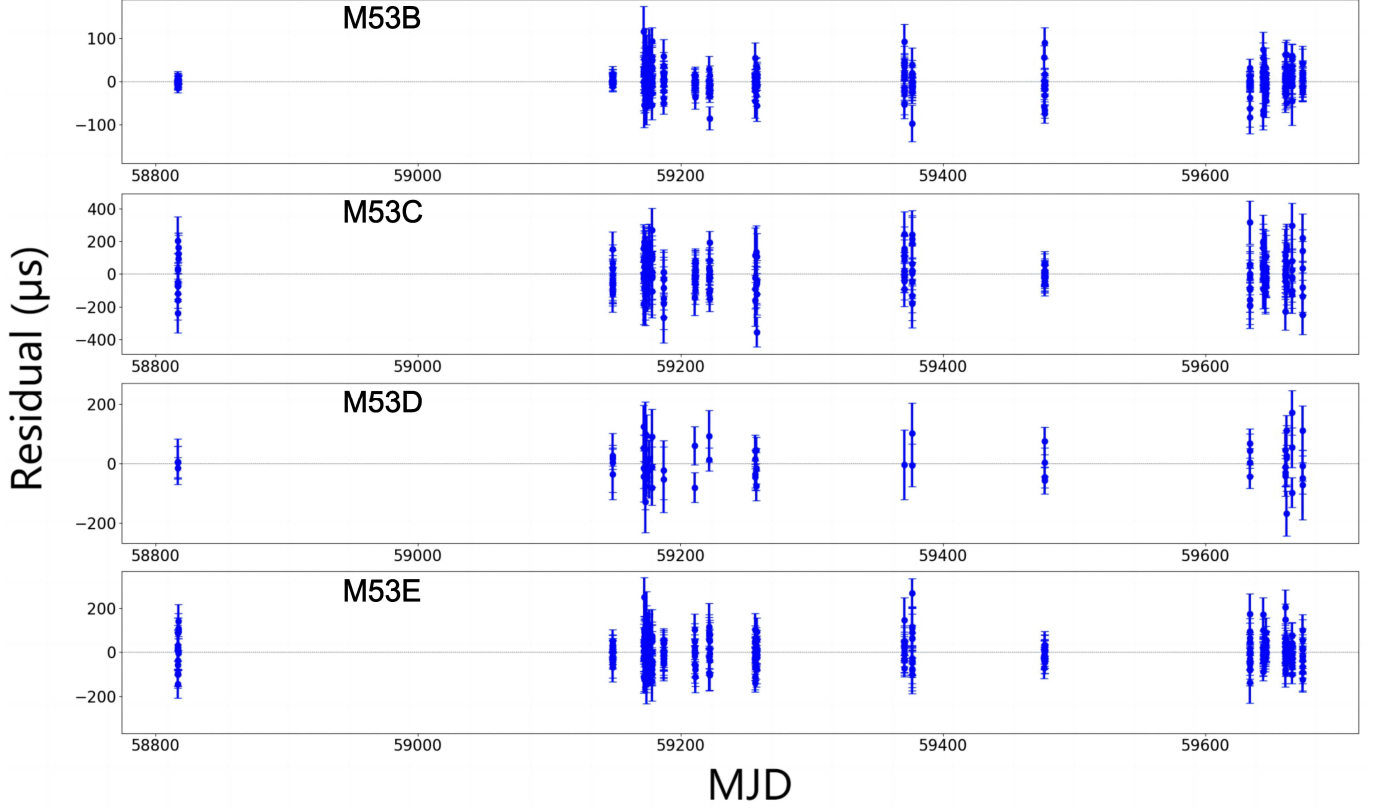


Figure 2. Timing residuals from the best-fit timing models presented in Table 2 as a function of the observation date for M53B to E.

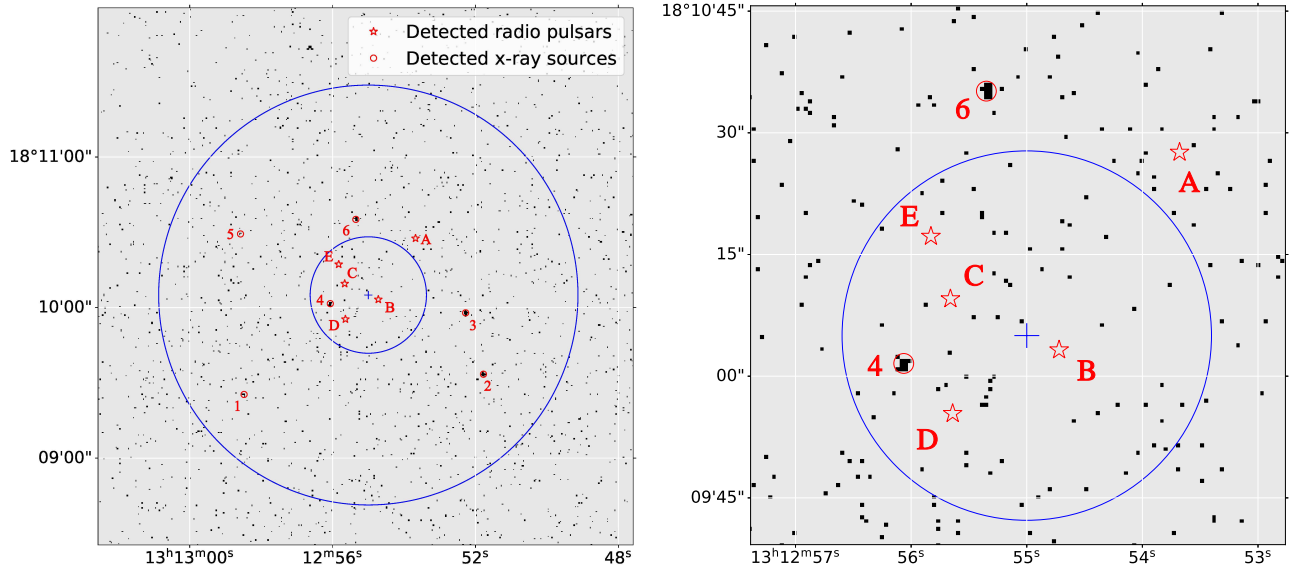


Figure 3. Positions of M53A to E, and six X-ray sources in M53, marked with red stars and circles respectively. The center of M53 is shown as a blue cross. **The position of M53A is from Lian et al. (in prep.).** The blue circles in the middle show a core radius ($0.35'$) and a half-light radius ($1.31'$). The background is the X-ray image of M53 from the *Chandra X-ray Observatory* archive (OBSID 6560). The left panel displays the details. For reference, the beam size of FAST is $3'$.

3.3×10^{31} to 7.6×10^{32} erg s⁻¹ in the band 0.3–8 keV, which lies above the estimated limiting luminosity of 3×10^{31} erg s⁻¹ (Zhao & Heinke 2022).

The X-ray emission of binary MSPs is observed to be both thermal and nonthermal character. For example, the X-ray radiation of most MSPs (at least 20 out of 29 MSPs) in 47 Tuc is well-defined by a thermal model, which is believed to originate from the magnetic polar caps of the underlying neutron star (Bogdanov et al. 2006; Bhattacharya et al. 2017). Alternatively, the nonthermal X-ray of B1957+20 and three radio eclipsing binaries MSPs 47 Tuc J, O, and W indicate the shock where the winds of the pulsar and its companion collide (Stappers et al. 2003; Bogdanov et al. 2006). Furthermore, in some more extreme cases, transient X-ray emission is produced by the accretion of matter from a low-mass companion star (e.g., see XTE J1808–369, Wijnands & van der Klis 1998). None of the binaries in M53 shows eclipses, so we'd generally expect only the thermal X-ray emission as in most pulsars in 47 Tuc. The non-detection of the M53 pulsars in the band 0.3–8 keV shows that their thermal X-ray emission is, when seen at the large distance of M53, too faint to be detectable in existing observations.

3.2. The single-binary encounter rate

The stellar encounter rate $\Gamma \propto \rho_c^2 r_c^3 / v$ (Verbunt 2003) is $\Gamma_{M4} = 0.84$ (where ρ_c is the central density of the GC, r_c is cluster core radius, v is the velocity dispersion, the result is normalized to the values of the GC M4, as in Verbunt & Freire 2014). The single-binary encounter rate ($\gamma_{M4} = \rho_c / v$) is 0.21. Γ ranks as the fourth lowest, and γ is the second lowest among the 38 GCs with known pulsars. M53 has four binary pulsars and one isolated pulsar, in this it is similar to the other GCs with a low γ_{M4} , which also have a high fraction of binary pulsars like M3 ($\gamma_{M4} = 0.6$, five binary pulsars), M13 ($\gamma_{M4} = 0.5$, four binaries and two isolated pulsars), and M71 ($\gamma_{M4} = 0.4$, five binary pulsars). This is consistent with the theoretical expectation that in clusters with a small γ_{M4} X-ray binaries are expected to evolve without much disturbance, forming binary MSPs similar to those of the Galactic disk. As noticed by Verbunt & Freire (2014), and confirmed several times since (e.g., in NGC 6624, Abbate et al. 2022 and the many isolated pulsars found in NGC 6517 by FAST mentioned in the Introduction), for the GCs with the largest values of γ_{M4} - the core-collapsed clusters - the situation is very different, with the population of detectable pul-

sars being dominated by isolated objects, a consequence of the high rates of orbital disruption.

3.3. Eccentricities of the M53 binary pulsars

During the formation of MSP-WD binaries, any eccentricity that the system might have prior to the low-mass X-ray binary phase will dissipate quickly from tidal circularisation, as observed in Galactic MSP binaries, for which the eccentricities follow the relation predicted by Phinney (1992). This means that the much larger orbital eccentricities observed for binary MSPs in globular clusters are likely due to gravitational perturbations of passing stars after accretion ceases (Rasio & Heggie 1995; Heggie & Rasio 1996).

In denser GCs, there will be many more encounters per unit time: for the example above, Terzan 5, the single binary encounter rate is $\gamma_{M4} = 13.0$, this means that within any time interval there is a ~ 62 times higher probability of a close encounter Terzan 5 compared to M53. This explains why the binaries in Terzan 5 have such high eccentricities (Prager et al. 2017; Martsen et al. 2022) compared to M53 where the orbits of the previous binary system (M53A) and the new binary pulsars are all mildly eccentric, with that of M53B having the largest eccentricity ($e = 0.013$).

For orbital periods of a few days to a few hundred days, Phinney (1992) predict eccentricities ranging from $\sim 10^{-6}$ to $\sim 10^{-3}$. The eccentricities of the binary systems in M53 are still significantly higher than this. Given the low stellar density of the cluster, it is important to verify whether the eccentricities of its binaries can arise from interactions with the stellar population of the cluster, which we do now. The time scale required to generate the eccentricity of M53B can be evaluated as (Rasio & Heggie 1995; Lynch et al. 2011):

$$t_{>e} \simeq 4 \times 10^{11} \text{ yr} \left(\frac{n}{10^4 \text{ pc}^{-3}} \right)^{-1} \left(\frac{v}{10 \text{ km s}^{-1}} \right) \times \left(\frac{P_b}{\text{days}} \right)^{-2/3} e^{2/5}, \quad (2)$$

where n is the number density of stars ($n \propto \rho_c$, ρ_c is the density of GC), v is the one-dimensional core velocity dispersion ($v = 4.4 \text{ km s}^{-1}$ for M53; Harris 2010), and P_b is the orbital period. Normalized with the values $\rho_c \sim 1.95 \times 10^5 \text{ L}_\odot \text{ pc}^{-3}$ and $n \approx 4.7 \times 10^5 \text{ pc}^{-3}$ of NGC 6517 (Lynch et al. 2011), the number density n is roughly estimated as $n \approx 2.6 \times 10^3 \text{ pc}^{-3}$, through the luminosity density of M53 ($\rho_c \sim 1.17 \times 10^3 \text{ L}_\odot \text{ pc}^{-3}$) reported in Harris (2010). These values imply $t_{>e} \approx 9.1 \times 10^9$ years, which is within the age of M53 $\sim 12.67 \text{ Gyr}$ (Forbes & Bridges 2010). We note that the lower limit for the characteristic age of M53B, discussed

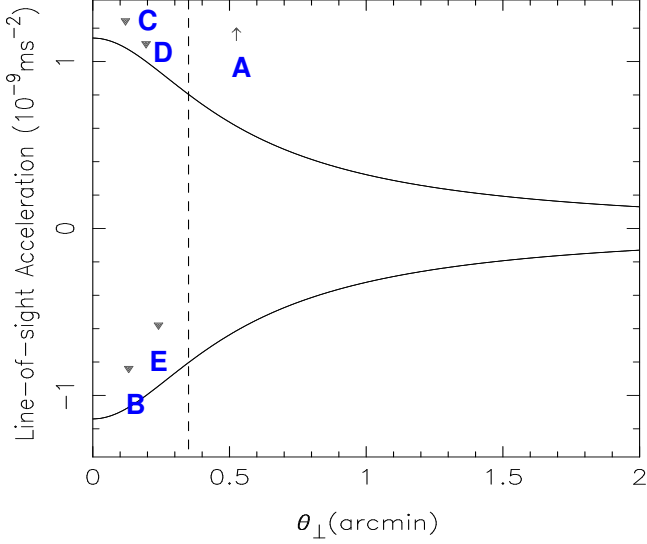


Figure 4. Acceleration model for M53. The black solid lines represent the upper and lower limits for the line-of-sight accelerations ($a_{\ell,GC}$) caused by the cluster as a function of the total angular offset from the centre of the cluster (θ_{\perp}). The triangles pointing down represent independent upper limits for the pulsar accelerations along the line of sight, $a_{\ell,P,\max}$. **The limit for M53A, from Lian et al. (in prep.), is well above the upper limit of this Figure.** The vertical dashed line represents the core radius. The cluster model can account for the negative \dot{P} values of M53B and M53E. The remaining pulsars are above that prediction, which is allowed since a_u has a contribution from their intrinsic spin period derivatives, which are positive.

below, is ~ 20 Gyr, a further indication that the pulsar is very old.

The eccentricities of M53D and M53E are fitted using the binary model ELL1 (Lange et al. 2001), both are below 10^{-4} . Although they are one order of magnitude larger than the prediction of Phinney (1992), they are smaller than expected for their orbital period and the density of their local environment. This could possibly be due to them either being younger than M53B or their orbits carrying them through less dense regions of M53.

3.4. Pulsar acceleration caused by cluster dynamics

In Table 2, we see that two of our discoveries (M53B and E) have negative \dot{P} . Since the intrinsic spin period derivative \dot{P}_{int} is positive for radio pulsars (which are generally spin powered), an observation of a negative \dot{P} suggests that the pulsar is accelerating in a gravitational field. The observed spin period derivative is generally given by:

$$\left(\frac{\dot{P}}{P}\right)_{\text{obs}} = \left(\frac{\dot{P}}{P}\right)_{\text{int}} + \frac{\mu^2 d}{c} + \frac{a_{\ell,GC}}{c} + \frac{a}{c}, \quad (3)$$

where μ is the total proper motion of the system, d is the distance to the cluster ($\mu^2 d/c$ is so-called the Shklovskii effect; see Shklovskii 1970), c is the speed of light, $a_{\ell,GC}$ is the line-of-sight acceleration of the pulsar in the gravitational field of the cluster, and a is the acceleration of the center of mass of the globular cluster in the potential of the Galaxy minus the Galactic acceleration of the Solar system projected along the line of sight from the Earth to M53.

Of these effects, two can be estimated with some precision: using the galactic rotation model developed by Prager et al. (2017), we obtain $a = 2.999 \times 10^{-12} \text{ m s}^{-2}$. The proper motions of the pulsars have not been measured yet, however, they should be very similar to that of M53, $0.042 \pm 0.08 \text{ mas yr}^{-1}$ (from *Gaia* DR2 data, Baumgardt & Hilker 2018); thus $\mu^2 d$ is $2.303 \times 10^{-14} \text{ m s}^{-2}$. Compared with the observed pulsar accelerations in M53 (e.g., $c\dot{P}_{\text{obs}}/P > -5.789 \times 10^{-10} \text{ m s}^{-2}$ for M53E), these effects are negligible.

The dominant term is the acceleration caused by the field of the GC, $a_{\ell,GC}$. To model this, we used an analytical model of the cluster described by Freire et al. (2005), which assumes the King (1962) density profile. With this, the accelerations due to the cluster potential at x (the distance from the pulsar to the centre of the GC divided by its core radius $r_c = \theta_c d$) can be calculated as:

$$a_{GC}(x) = \frac{9\sigma^2}{d\theta_c} \frac{1}{x^2} \left(\frac{x}{\sqrt{1+x^2}} - \sinh^{-1} x \right). \quad (4)$$

The parameters for this model include the position and distance of M53 (see section 1), its core radius ($\theta_c = 0.35'$; Harris 2010), and the central stellar velocity dispersion ($\sigma \sim 6.5 \text{ km s}^{-1}$)⁸. The values for the line-of-sight component $a_{\ell,GC}(x)$ can be calculated by multiplying $a_{GC}(x)$ by ℓ/x , where ℓ is the distance (also in core radii) to the plane of the sky that passes through the centre of the cluster. In Fig. 4, the solid black curves represent the maximum and minimum values of $a_{\ell,GC}(x)$ for each line of sight through the cluster, which is characterized by a constant angular offset from the centre, θ_{\perp} .

For all pulsars, we can derive an independent upper limit on the acceleration from \dot{P}_{obs} :

$$a_{\ell,P,\max} = c \frac{\dot{P}_{\text{obs}}}{P} \quad (5)$$

Fig. 4 graphically shows the constraints for each pulsar in M53 as the triangles pointing down, which highlights

⁸ <https://people.smp.uq.edu.au/HolgerBaumgardt/globular/>

Pulsar name	$a_{\ell, P, \max}$ 10^{-9} m s^{-2}	$a_{\ell, \max}$ 10^{-9} m s^{-2}	\dot{P}_{int} $10^{-20} \text{ s s}^{-1}$	B 10^9 G	τ_c Gyr
M53B	-0.84	1.07	<0.48	<0.18	>20.45
M53C	1.24	1.08	0.68 ~ 9.72	0.29 - 1.11	29 - 2.04
M53D	1.11	1.00	0.22 ~ 4.26	0.12 - 0.51	45 - 2.26
M53E	-0.58	0.94	<0.48	<0.14	>13.03

Table 3. For each of the new pulsars in M53, we calculate the upper limit for the pulsar accelerations, the upper and lower limits for the line-of-sight pulsar acceleration due to the cluster potential and the resulting limits on the intrinsic spin period derivative, the surface magnetic field strength (B), and the characteristic age (τ_c) respectively.

that they are upper limits on the cluster acceleration that assume $\dot{P}_{\text{int}} = 0$. These also presented in Table 3.

From this figure, we conclude that, despite the small accelerations predicted by the analytical model described above, it can account for the negative \dot{P}_{obs} of M53B and E. It cannot fully account for the positive $a_{\ell, P, \max}$ of the remaining pulsars, but this is to be expected because their spin-down has a contribution from a positive \dot{P}_{int} .

Taking the maximum and minimum accelerations caused by the gravitational field of the GC for the line of sight of each pulsar, we can calculate maximum (and in some cases minimum) limits for the \dot{P}_{int} of each pulsar; from these we can calculate maximum (and in some cases minimum) values for their magnetic fields and minimum (and in some case maximum) values for their characteristic ages. These values are presented in Table 3.

From these values, it is clear that all new pulsars in M53 have weak magnetic fields and are very old, all with characteristic ages larger than 2 Gyr. This makes them, again, similar to the MSP population observed in the Galactic disk, as predicted by the low γ_{M4} .

4. CONCLUSIONS

In this paper, we present the discovery of M53E during the monitoring observations. With 22 FAST observations from 2019.11 to 2022.04, we have obtained timing solutions of M53B to E, these were only possible owing to the high sensitivity of the radio telescope. All of these are millisecond pulsars; M53C is the only isolated pulsar known in M53. Based on the orbital characteristics, the orbiting companions for M53B, D, and E are most likely white dwarf stars with masses of 0.25, 0.27, and 0.18 M_{\odot} , respectively. All of them have low orbital eccentricities.

Two of the new pulsars have negative \dot{P}_{obs} . Using an analytical cluster potential model for M53 (see e.g., Freire et al. 2005), we see that, despite its small predicted accelerations, it can account for those \dot{P}_{obs} . We conclude, additionally, that all four pulsars have magnetic fields of the order of, or smaller than, 10^9 G and characteristic ages of several Gyr.

None of the bright X-ray sources detected with the achieved *Chandra X-ray Observatory* observations correspond to the positions of these four MSPs, no significant new sources are detectable at their positions.

The pulsar population of M53 has the characteristics expected for a GC with a low single-binary encounter rate γ_{M4} , i.e., that they originate in X-ray binaries that evolved to MSP binaries without disturbance. This population thus resembles the MSP population in the Galactic disk: 1) The fraction of single pulsars is small (one isolated pulsar for four binary pulsars), 2) low eccentricity orbits (which are nevertheless slightly perturbed by nearby encounters, especially for the wider binaries, as expected) and 3) small magnetic fields and large characteristic ages. This population contrasts with that of GCs with higher γ_{M4} , where we see many more isolated pulsars, high-eccentricity binaries and apparently young pulsars (Abbate et al. 2022), which can form there from the disruption of X-ray binaries (Verbunt & Freire 2014).

With the ongoing FAST observations on M53, we **have obtained a unique timing solution for M53A, and have extended it to the past using Arecibo observations, we now have a 32-year timing baseline for this pulsar. Additional FAST and processing of additional Arecibo observations will further improve this timing solution (Lian et al., in prep.)**. We will also extend the timing solutions of M53B to E into the future. This will eventually allow the measurement of proper motions and possibly the orbital period derivatives, which will provide independent measurements of the pulsar accelerations. The precise positions of the pulsars will allow optical and X-ray follow-up of these systems; this will be made easier by the lower-than-usual stellar density of this globular cluster, which will make the unambiguous identification of companion stars easier.

ACKNOWLEDGEMENTS

This work is supported by the National Natural Science Foundation of China (Nos. 12041301, 12021003, 11633001, and 11920101003). This work made use of the

data from FAST (Five-hundred-meter Aperture Spherical Radio Telescope). FAST is a Chinese national mega-

science facility, operated by the National Astronomical Observatories, Chinese Academy of Sciences.

REFERENCES

- Abbate F., Ridolfi A., Barr E. D., Buchner S., Burgay M., Champion D. J., Chen W., et al., 2022, *MNRAS*, 513, 2292
- Andersen, B. C., & Ransom, S. M. 2018, *ApJL*, 863, L13
- Baumgardt, H., Hilker, M., 2018, *MNRAS*, 478, 1520
- Bhattacharya, D., & van den Heuvel, E. P. J. 1991, *PhR*, 203, 1
- Bhattacharya, S., Heinke, C. O., Chugunov, A. I., et al. 2017, *MNRAS*, 472, 3706
- Bogdanov, S., Grindlay, J. E., Heinke, C. O., et al. 2006, *ApJ*, 646, 1104
- Camilo, F., Lorimer, D. R., Freire, P., Lyne, A. G., & Manchester, R. N. 2000, *ApJ*, 535, 975
- Camilo, F. & Rasio, F. A. 2005, in *Astronomical Society of the Pacific Conference Series*, Vol. 328, *Binary Radio Pulsars*, ed. F. A. Rasio & I. H. Stairs, 147
- Clark, G. W., 1975, *ApJ*, 199, L143
- Forbes, D. A., & Bridges, T. 2010, *MNRAS*, 404, 1203
- Freire, P. C., Kramer, M., Lyne, A. G., 2001, *MNRAS*, 322, 885
- Freire, P. C., Gupta, Y., Ransom, S. M., & Ishwara-Chandra, C. H. 2004, *ApJ*, 606, 53
- Freire, P. C. C., Hessels, J. W. T., Nice D. J., Ransom, S. M., Lorimer, D. R., Stairs, I. H., 2005, *ApJ*, 621, 959
- Freire, P. C. C., Ridolfi, A., Kramer, M., et al., 2017, *MNRAS*, 471, 857
- Freire, P. C. C., & Ridolfi, A. 2018, *MNRAS*, 476, 4794
- Harris, W. E., 1996, *AJ*, 112, 1487
- Harris, W. E. 2010, *arXiv:1012.3224*
- Heggie, D. C., & Rasio, F. A., 1996, *MNRAS*, 282, 1064
- Hessels, J. W. T., Ransom, S. M., Stairs, I. H., et al. 2006, *Sci*, 1311, 1901
- Hessels, J. W. T., Ransom, S. M., Stairs, I. H., Kaspi, V. M., & Freire, P. C. C. 2007, *ApJ*, 670, 363
- Jiang, P., Yue, Y., Gan, H., et al. 2019, *SCPMA*, 62, 959502
- Jiang, P., Tang, N.-Y., Hou, L.-G., et al. 2020, *RAA*, 20, 064
- Katz, J. I., 1975, *Nature*, 253, 698
- King, I., 1962, *AJ*, 67, 471
- Kulkarni, S. R., Anderson, S. B., Prince, T. A., & Wolszczan, A. 1991, *Natur*, 349, 47
- Lange, C., Camilo, F., Wex, N., et al., 2001, *MNRAS*, 326, 274
- Lorimer, D. R., 2008, *LRR*, 11, 8
- Lorimer, D. R., & Kramer, M., 2004, *Handbook of Pulsar Astronomy*, Vol. 4 (Cambridge: Cambridge Univ. Press)
- Lynch, R. S., Ransom, S. M., Freire, P. C. C., & Stairs, I. H., 2011, *ApJ*, 734, 89L
- Lyne, A. G., Brinklow, A., Middleditch, J., Kulkarni, S. R., Backer, D. C., 1987, *Nature*, 328, 399
- Manchester, R. N., Lyne, A. G., Robinson, C., et al. 1991, *Natur*, 352, 219
- Manchester, R. N., Hobbs, G. B., Teoh, A., & Hobbs, M. 2005, *AJ*, 129, 1993
- Martsen, A. R., et al., 2022, *arXiv e-prints*, p. [arXiv:2204.06158](https://arxiv.org/abs/2204.06158)
- Nan, R., Li, D., Jin, C., et al. 2011, *IJMPD*, 20, 989N
- Nice, D., Demorest, P., Stairs, I., et al. 2015, *Tempo: Pulsar Timing Data Analysis*, *Astrophysics Source Code Library*, [ascl:1509.002](https://www.ascl.net/asn/ascl:1509.002)
- Pan, Z., Hobbs, G., Li, D., et al. 2016, *MNRAS*, 459L, 26P
- Pan, Z., Ransom, S. M., Lorimer, D. R., et al. 2020, *ApJ*, 892L, 6P
- Pan, Z., et al., 2021b, *ApJ*, 915, L28
- Phinney E. S., 1992, *Philosophical Transactions of the Royal Society of London Series A*, 341, 39.
- Prager, B. J., Ransom, S. M., Freire, P. C. C., et al. 2017, *ApJ*, 845, 148
- Ransom, S. M. 2001, PhD thesis, Harvard Univ., http://www.cv.nrao.edu/~sransom/ransom_thesis.2001.pdf
- Ransom, S. M., Eikenberry, S. S., & Middleditch, J. 2002, *AJ*, 124, 1788
- Ransom, S. M., Cordes, J. M., & Eikenberry, S. S. 2003, *ApJ*, 589, 911
- Ransom, S. M., Hessels, J. W. T., Stairs, I. H., et al. 2005, *Sci*, 307, 892
- Rasio, F. A., & Heggie, D. C., 1995, *ApJ*, 445, L133
- Ridolfi, A., Freire, P. C. C., Gupta, Y., & Ransom, S. M., 2019, *MNRAS*, 490, 3860
- Ridolfi, A., Gautam, T., Freire, P. C. C., et al. 2021, *MNRAS*, 504, 1407
- Robinson, C., Lyne, A. G., Manchester, R. N., et al. 1995, *MNRAS*, 274, 547
- Shklovskii, I. S., 1970, *Soviet Ast.*, 13, 562
- Sigurdsson, S. & Phinney, E. S., 1993, *ApJ*, 415, 631
- Stappers, B. W., Gaensler, B. M., Kaspi, V. M., van der Klis, M., & Lewin, W. H. G. 2003, *Science*, 299, 1372
- Verbunt, F. 2003, in *New horizons in globular cluster astronomy*, eds. G. Piotto et al., *ASP Conf. Ser.*, 296, 245

Verbunt, F., Freire, P. C. C., 2014, *A&A*, 561, A11

Wang, L. et al., 2020, *ApJ*, 892, 43

Wijnands, R., & van der Klis, M. 1998, *Natur*, 394, 344

Yan, Z., Pan, Z., Ransom, S. M., et al. 2021, *ApJ*, 921, 120

Zhao, J., & Heinke, C. O., 2022, *MNRAS*, 511, 5964